International Journal of Computing and Digital Systems
ISSN (2210-142X)
Int. J. Com. Dig. Sys. 15, No.1 (Feb-24)

http://dx.doi.org/10.12785/ijcds/150166

A Cooperative Relaxation-Based Method for Range Image Segmentation

Imene Belloum[1], Mourad Bouzenada[1] and Smaine Mazouzi[2]

[1]*Department of computer science, Université Abdelhamid Mehri Constantine 2, Constantine, Algeria*
[2]*Department of computer science, Université 20 Août 1955, Skikda, Algeria*

Received 7 Jul. 2023, Revised 28 Jan. 2024, Accepted 31 Jan. 2024, Published 5 Feb. 2024

Abstract: In range images, edge detection is a hard task because of high levels of noise and distortions, produced at image acquisition. However, detecting edges in range image allows to enhance region-based segmentation, which is a key step for any further step in image analysis and understanding. To deal with the hard problem of range image segmentation, we propose in this paper a combination of an edge-based and a region-based methods for the segmentation of noisy and distorted real range images. The proposed combination is based on the relaxation of the detection results of both edges and regions. For region-based segmentation we have proposed a new multi-seed region growing algorithm using curvature as homogeneity criterion. For edge-based segmentation, we have detector adapted the Canny filter by taking into account a vectorial representation of raw data in range images. So, the two resulted sets of edges are obtained from two different representations of the same image data. The principle of the introduced method consists in matching the two segmentation results as a mutual self-regularization, and whose objective is to produce an optimal final segmentation with respect to a given criterion of optimality, expressed by a well appropriate energy-based objective function. The optimal solution, considered as unique, is calculated by the simulated annealing algorithm, and consists of the best edge map that can obtained on the processed range images. The experimental results, using the ABW database, show better results compared to those obtained by the classical Canny detector. So, we can conclude that the proposed relaxation-based combination allows more efficient segmentation of range images.

Keywords: Range Image,Edge detection, Region-based segmentation, Relaxation.

1. Introduction

Increased availability and low cost of range images that have followed the commercialization of Kinect scanners [1], has allowed easy access to this type of images, and has seen the emergence of a new family of methods for processing this kind of images, aiming at providing an unambiguous representation of the observed scenes [2], unlike 2D images, where visual 2D data do not allow well understanding the geometry of the observed objects. The combination of various representations of image data allows the improvement of the processing results of this type of images, including the segmentation results. Obviously, the availability of labelled data has allowed the appearance of a large number of works that have used machine learning techniques for image segmentation in general and range images in particular [2], known as semantic or object-oriented segmentation. However, scaling up for this type of method is not easy; the fact that the images to be processed may not have common characteristics with those having served as training data [3]. It is therefore still necessary to propose model-based or heuristic-based methods for the segmentation of images, including range images. For this kind of images, edge detection, which can be very helpful for further processing, it is hard to perform, because of noise and distortions that are high in such images.

In this work, aiming at efficiently segmenting range images, we propose a cooperative relaxation-based range image segmentation method. Its principle consists in matching the detection results obtained on the basis of two different representations of the images: representation oriented edge detection, and representation oriented region segmentation. For the latter, we perform a region-growing using Gaussian curvature [4] as homogeneity criterion. The borders of the resulting regions are considered for matching with the results of segmentation by edge detection, obtained by a Canny filter adapted to range images [5]. The obtained two border maps are matched for mutual self-regulation by relaxation based on an introduced objective function, well suited for this purpose. Relaxation allows simultaneously improving the edge map of the processed image. The final result is optimal with respect to the objective function, and is obtained by minimization of the latter using a meta-heuristic, namely simulated-annealing. We conducted experiments using a well-known range image database ABW [6]. The obtained results showed the interest of the proposed

E-mail address: imene.belloum@univ-constantine2.dz, mourad.bouzenada@univ-constantine2.dz, s.mazouzi@univ-skikda.dz

method to produce an accurate edge map that allows reliable segmentation of this type of image.

The remainder of the paper is organized as follows: In section 2, we present a short state of the art of range image segmentation methods, including those having used range data from RGB-D images. Section 3 is devoted to the proposed method where we show region-based segmentation and edge detection in range images using two different representations. We also show how the results are combined using a self-regularization principle based on relaxation. The experimental results are presented in section 4, and will be followed by an analysis and a discussion. Finally, a conclusion summarizes our work and outlines its potential perspectives.

2. Related Work

A. Range Images

A range image is a three-dimensional representation of a real scene, captured by a device, usually active and laser-based. It is a matrix of pixels, where at a given pixel (x, y) is stored the depth, representing the distance from this point to a given observer. The range image is not intended to be seen by a human being, because what it contains are not colors or gray levels but distances. This feature, as well as the high level of noise in this type of image, makes it difficult to process, especially to segment. For three decades, dozens of methods have been proposed [7] without any of them being able to effectively segment this type of images unlike for methods that process color or gray level images, where segmentation is usually efficient.

B. Range Image Segmentation Methods

Since several decades, and in order to provide reliable and real-time vision systems, numerous authors have proposed different methods and architectural models for range image segmentation. Poppinga et al.[8] deal with incremental aspect in 3D range image segmentation. They proceed by optimally select neighbor pixels when the region growing is performed, and where the plan equation is incrementally updated after each pixel is included to the region. Aiming to provide a fast range image segmentation, Holz and Behnke [9] introduced a novel method that compute surface meshes, plan equations, and curvatures. After that a region growing is applied to the resulted features in order to produce a region based image segmentation. Aiming at providing a navigation system for autonomous robots, Stuckler et al. [10] proposed a segmentation algorithm that uses surface normals as features and where they are computed by fitting the best tangent plans. An unsupervised clustering on computed normal vectors allows generating the whole image segmentation. Buyssens et al. [11] used superpixels with range images aiming to enhance segmentation performance, namely the accuracy. Indded, in addition to performance purpose, it has been noticed in different papers that using superpixels to reduce the complexity of computation, mainly in low-level image processing, including image segmentation [12].

For more than ten years, several authors have proposed different techniques for indoor scene understanding and analysis with promising results where they used range data, extracted from RGB-D images [13], [14], [15] and [16]. The latter are formed by two aggregated images, one containing color data and the second the depths of observed points of the scene. Some of these researches incorporate depth as complementary information with color images. Extraction of various features, kernel design, and pixel classification using trained classifiers are typical approaches to the RGB-D scene analysis problem. As a sample, [15] suggested contextual models in a supervised environment. Their model combines a segmentation tree and a superpixel Markov Random Field with kernel descriptors (MRF). To do this, they added the global probability of borders (gPb) of range image to the well-known gPb-UCM algorithm [17]. By applying watershed to the gPb of the RGB image, the RGB-D scene analysis approach provided initially by [16] produces an over segmentation of the scene. The over-segmentation is then aligned with the 3D plans. Finally, They apply a hierarchical segmentation to integrate regions using a trained classifier. The gPb-UCM [17] approach was recently expanded by [14] to include supervised settings. First, they integrate monocular signals like as brightness, color, and texture with geometric contour cues such as convex and concave normal gradients. Then, using learned classifiers for 8 distinct orientations, they identify pixels as contours. Recently, semantic segmentation has been successfully applied to RGB-D image segmentation, as shown in [18] where the authors improved a previous deep learning-based model aiming at reducing the model parameters. So, they were able to produce a hierarchy of segmentations from all oriented detectors. Each of the strategies listed above employs a supervised approach to merge or fuse various attributes or information obtained from them. In [13], authors examined the unsupervised setting-based fusion of color and geometry and provided a solution utilizing the normalized cut spectral clustering algorithm. Their strategy entails choosing the best multiplier to strike a balance between depth and color. The method described by the authors in [19] involves first extracting the edges from an RGB image, applying Delaunay Triangulation to the edges to create a triangular graph, what allows finally the use of Normalized Cut Algorithm. In a subsequent stage, they use RANSAC [20] to extract planar surfaces from the segments, and then they merge the coplanar segments by employing a greedy merging technique. In addition to these strategies, joint color and depth picture segmentation is added to the well-known graph-based segmentation [21]. For instance, [22] expanded it to include color disparity in order to segment stereopsis images. The graph-based approach was expanded in [23] by the incorporation of surface normals to segment colored 3D laser point clouds. An other developed model called Scene-SIRFS [24] seeks to extract fundamental scene features from a single RGB-D image. It takes into account a combination of shapes and illuminations where the combination consists of are encapsulated in a 17-eigenvector soft segmentation. These eigenvectors are derived from the input

RGB image's normalized Laplacian. A method for RGB-D image semantic segmentation based on the interactive conditional random field was proposed in [25]. Authors of this work claim that this method may be successfully used to segment complicated and varied real-world situations. In this study, the conditional random field approach was used to approximately segment the image with the goal of reducing image noise and data loss. Morphological reconstruction methods were then employed to enhance the segmentation result using a platform for human-computer interaction. Stuckler et al. [26], who also recover object segmentation and motion simultaneously using a piecewise rigid motion model and energy minimization. Shaoguo Liu proposed a new energy minimization method to fill the missing regions and remove noise in a range image [27].

Recently, some authors used unsupervized approaches to segment 3D point Clouds. Zihui Zhang et al. [28] proposed an unsupervised semantic segmentation of 3D point clouds that they call GrowSP. Their principle consists in discovering 3D semantic parts by incrementally growing points. The proposed method proceeds in three main steps, 1) feature extracting to learn per-point features, 2) Superpoint constructing to incimentally grow the superpoints, and 3) Semantic primitive clustering to merge superpoints in order to obtain semantic elements. Moreover, region rowing-based segmentation still be used, in particular for 3D point cloud segmentation. Yu et al. have introduecd a curvature-based region growing for 3D point cloud segmentation [29]. The seed selection issue was resolved by considering the point with the smallest curvature as the region seed. A confidence interval is calculated according angles between surface normals then used to assimilate points to the regions.

We have noticed that most of recent methods are machine-learning based, which make them very computationally complexes. Furthermore, they used one or more data modalities, but never several representations. We introduce in this paper a novel cooperative relaxation-based method that exploits two different representations of range data in order to enhance range image segmentation.

3. A Relaxation-Based Method for Range Image Segmentation

A. Principle

First, two segmentations are produced independently of each other, and this by using for each a different representation of the data of the image, namely a region-oriented representation and an edge-oriented one. With the first representation, we perform an extraction of the different regions of the image based on a new multi-seed region growing, and by considering the Gaussian curvature as a criterion of homogeneity. Next, a map of the edges obtained from the borders of the extracted regions is calculated, and which will be matched subsequently to the map of edges, obtained from the second representation. So the two basic techniques, respectively edge-based and region-based are cooperatively employed on the basis of relaxation in order to enhance the final edge map of the image.

Edge detection is performed using the plan equation parameters, adjusted locally at the level of image pixels. Unlike 2D images, the gradient that will allow the detection criterion will be calculated as the difference of the parameters of the corresponding equations of the plans. Finally, the two maps, respectively of region borders and of detected edges, are matched in order to produce a final edge map, what allows to precisely delimiting the objects appearing in the image. The following figure (Fig. 1) shows the principle of the proposed method.

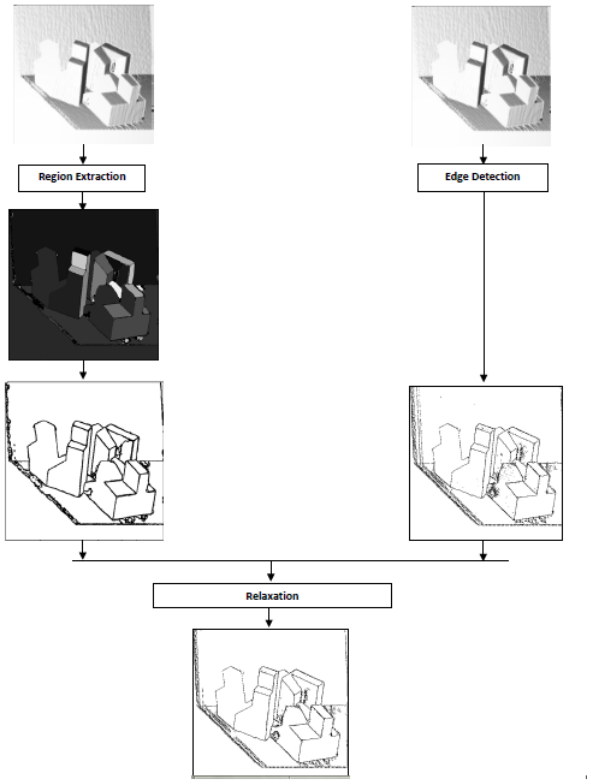

Figure 1. Principle of segmentation of range images by relaxation

B. Multi-Seed Region Growing

We use the Gaussian curvature expressed by formula 1, as a criterion of homogeneity for the region growing in range images, where recorded depths are scalar values, ranged between 0 and 255. The growing of regions begins with a random selection of a set of seeds in the image. However, a seed is accepted for growth if its neighbourhood consists of a homogeneous local region of the image. Therefore, we calculate the standard deviation of the curvatures in the neighbourhood of the seed, and the latter is accepted to continue the growing if this standard deviation is lower than a certain threshold T_σ, expressing the fact that this local region is homogeneous.

The Gaussian curvature K at point (x, y) of the image d, is expressed as follows:

$$K = \frac{I''_{xx} I''_{yy} - I''^2_{xy}}{\left(1 + I'^2_x + I'^2_y\right)^2} \quad (1)$$

Where I'_x, I'_y, I''_{xx}, I''_{yy}, I''_{xy} are the partial derivatives of order 1 and order 2 in the x and y directions. For range images containing only polyhedral objects, the curvature should be null inside the surfaces, which are in this case flat, and therefore the numerator of the curvature expression is sufficient to characterize homogeneous pixels (belonging to the same plan). At the end of the growing of the regions that having started from different seeds, the different obtained sub-regions are merged, and thus the final region-based segmentation is obtained. The following algorithm shows the multi-seed region growing algorithm.

Algorithm Multi-seed increase

Algorithm 1 Multi-seed growing

Input:*Range image*,T_σ,*min_seeds*,*max_seeds*
Output: *all regions*
BEGIN
for *i* ranging from 1 to number of seeds **do**
repeat
$(xg, yg) \leftarrow (random(image.width), random(image.height))$
$\delta_k \leftarrow$ *standard deviation of curvatures of neighboring pixels of (xg,yg)*
until $\delta_k \leq T_\sigma$
$region_i \leftarrow Increasefrom(xg, yg)$
end for
$numberofregions \leftarrow numberofseeds$
repeat
*region*1 ← *random*(*numberofregions*)
*region*2 ← *random*(*numberofregions*)
if (region1 ≠ region2) AND *(region1 adjacent to region2)* AND $|averageofcurvaturesofregion1 - averageof$ *curvatures of region2*$| < T_m$ **then**
new region ← *merge region 1 and region 2*
delete region1
delete region2
add new region
number of regions ← *number of regions -1*
end if
until *number of regions unchanged for a long time*
END.

T_m and T_σ are respectively the mean and standard deviation thresholds of the curvatures K of the surfaces. They will be initialized experimentally using a subset of training images (see 4). After extracting the regions, all of their borders are extracted, in order to be latter matched to the set of edges, detected by Canny detector.

C. Edge Detection

As the image data are not colors or gray levels, it is not efficient to proceed by calculating the gradient of depths and use it with the Canny algorithm. Indeed, discontinuities can exist in the depth data without the corresponding points being edge points [7]. As a result, we took a vectorial representation of the image data by calculating at each pixel of the image the equation of the plan [30], then using the deviation of the parameters as the magnitude of the gradient. The other stages remain the same as Canny detector for gray level images [5], and which can be summarized as follows:

1) Noise smoothing, using a Gaussian filter, with $\sigma = 1.6$ and a convolution mask of size 5x5.

2) Calculation of the gradient image using the Sobel operator, where at each pixel (x, y) are stored the norm of the gradient, and its direction, expressed by the angle of the gradient vector with the X axis.

3) Removal of pixels whose gradient norms are less than the local maximum, in the direction of the gradient vector.

4) Hysteresis thresholding of the edge points obtained in the previous steps, by using two adequate thresholds.

D. Relaxation-Based Edge Matching

First, it should be noted that several edges detected by Canny are to be discarded, because they are located inside the surfaces of the objects, and do not correspond to any borders of the surfaces. In fact, the surface borders are the only true edges in the range images. Thus, any detected edge by Canny and is located far from the region borders in the depth image is simply discarded. After removing such edges, the resulting edge maps from the two segmentation methods are relaxed. Let us denote by C_1, and C_2 the edge maps obtained respectively by the extraction of the borders from the segmentation of the image by region growing and by the edge detection using Canny algorithm.

1) Removing False Edges

The edge points from C_2 whose minimum distance to all of the edges points of C_1 are simply deleted. These edge points are due to significant deformations of the data during acquisition, especially when the corresponding surfaces are not exposed to the observer (laser detector). The following algorithm shows how this set of points is removed from the C_2 set.

Algorithm Remove from C_2

Algorithm 2 Remove_from_C_2

Input: Sets C_1, C_2
Distance threshold T_d
Output: C_2
BEGIN
for any point p in C_2 **do**
  $min\_distance \leftarrow \infty$
  for any point q in C_1 **do**
    if distance (p, q) < min_distance **then**
      $min\_distance \leftarrow distance(p, q)$
    end if
  end for
end for
if min_distance < T_d **then**
  Remove p from C_2
end if
END.

2) Removing Of Noise Edges In The Range Image

These are points erroneously detected as edge points according to the representation by region, due to noise regions. It is possible that a whole region of noise in the depth image is detected as a homogeneous region, and therefore its equivalent does not appear in the edge representation image. The following algorithm shows how the edges of these regions are removed from the set C_1.

Algorithm Remove from C_1

Algorithm 3 Remove_from_C_1

Input: Sets C_1, C_2
Distance threshold T_d
Output: C_1
BEGIN
for any point p in C_1 **do**
  $min\_distance \leftarrow \infty$
  for any point q in C_2 **do**
    if distance (p, q) < min_distance **then**
      $min\_distance \leftarrow distance(p, q)$
    end if
  end for
end for
if min_distance < T_d **then**
  Remove p from C_1
end if
END.

3) Energy Function For The Relaxation On The Sets C_1 and C_2

We express the energy function as a sum of two opposing energies. The first is an internal energy noted E^i expressing the a priori that the two sets of contours are identical in ideal conditions. The second is the external energy, denoted E^e expressing the adequacy of the detection with respect to the image data. The overall energy is weighted sum of the previous energies: $E = E^i + \lambda E^e$.

Initially E^i is maximal expressing the difference which exists between the two sets C_1 and C_2. The objective of the relaxation is to minimize this energy E^i, under the constraint of not highly raising the external energy E^e . The latter is zero at the start of the relaxation, expressing the adequacy of the detection with respect to the image data. Then, it will be increased according to the alteration of sets C_1 and C_2, where the energy E^i is at the same time reduced. We consider that the optimum of the energy function E represents a balanced detection between the two representations "Regions" and "Edges". The factor λ is used to balance E^i and E^e because the latter are expressed according to different data (distances on the one hand, and norm of the gradient and curvatures of Gauss on the other hand). This parameter will be initialized experimentally.

E^i is expressed as the sum of the distances between the points of set C_1 and the closest points of set C_2. Note that E^i is zero in the case of superposition of the two sets C_1 and C_2.

$$E^i(C_1, C_2) = \sum_{p \in C_1} \min_{q \in C_2} \{d(p, q)\} \tag{2}$$

E^e is expressed as a function of the norms of the gradient vectors of the points in the set C_2 and of the Gaussian curvatures of the set C_1:

$$E^e(C_1, C_2) = A + B - \sum_{p \in C_1} \left[K_p\right] - \sum_{q \in C_2} \left[\overrightarrow{\nabla}_q\right] \tag{3}$$

With

$$A = \sum_{p \in C_1^0} \left[K_p\right] \tag{4}$$

And

$$B = \sum_{q \in C_2^0} \left|\overrightarrow{\nabla}_q\right| \tag{5}$$

Where

C_1^0 and C_2^0 are respectively the initial subsets of C_1 and C_2, obtained by increasing regions, and by detecting edges. Note that E^e is zero at the beginning of the relaxation $\left(C_1 = C_1^0, C_2 = C_2^0\right)$.

Formally, the optimal edge map of the processed image, can be expressed as follows:

$$C = C_1 \cup C_2 = \arg\max_{C_1,C_2}\{\sum_{p\in C_1}\min_{q\in C_2}\{d(p,q)\} + A + B - \sum_{p\in C_1}\left[K_p\right] - \sum_{q\in C_2}\left[\overrightarrow{\nabla_q}\right]\} \quad (6)$$

4) Optimal Computing of Solution

The objective function E, is complex and concave, depending on a large number of variables points of the subsets C_1 and C_2, we opted for the meta heuristic of simulated annealing to calculate the minimum of E, and so obtain the optimal solution, expressed by the resulting subsets C_1 and C_2. In this case a solution S is expressed by the pair of subsets (C_1,C_2). A neighboring solution S' of S is obtained by randomly and locally modifying the position of a subset $C \subset C_1 \cup C_2$.

The following algorithm is the application of the simulated annealing metaheuristic Algorithm Relaxation-By-Simulated Annealing

Algorithm 4 Relaxation-By-Simulated Annealing

Input: Sets C_1, C_2
Output: C
BEGIN
$C \leftarrow C_1 \cup C_2$
$T = 1$
while C still changes **do**
  Randomly get a point $p(x, y)$ from C
  $x \leftarrow x + (1 - 2 \times random)$
  $y \leftarrow y + (1 - 2 \times random)$
  if $p \in C_1$ **then**
    $C'_1 \leftarrow C_1/\{p\} \cup \{(x, y)\}$
  else
    $C'_2 \leftarrow C_2/\{p\} \cup \{(x, y)\}$
  end if
  if $(E(C'_1, C'_2) < E(C_1, C_2))$ OR $(random < e^{-\delta\times T})$ **then**
    // accept the new solution
    $C_1 \leftarrow C'_1$
    $C_2 \leftarrow C'_2$
  end if
  $T = (1 - \delta) \times T$
end while
// The final contour is $C_1 \cup C_2$
END.

4. Experimentation

We considered the ABW range image database [6], which is widely used for range image segmentation. The database contains 10 training images, initially used to estimate the parameters of the segmentation methods involved in the comparative study provided by Hoover et al. [6], and 30 test images with their ground truth segmentation, for the evaluation of the methods. The performance criteria differ according to the methods, their principles and their objectives. For the region-based segmentation methods, the 4 criteria adopted by the authors of this type of methods are: the number of correctly detected regions, the number of under-segmented regions, the number of over-segmented regions and the noise regions. However, for edge-based methods, such as ours, several metrics could be used such as Precision and Dice index [31].

A. Parameter Selection

The 10 training images are used to adjust the parameters of the method, namely T_m, T_σ, T_d, and λ, respectively thresholds of the average of the curvatures, threshold of the standard deviation of the curvatures and the threshold of the minimum distances (used by removing algorithms of the points of the two sets C_1 and C_2), and the external energy weight. We varied the values of the 4 parameters, and we keep the values corresponding to the maximum of correctly detection expressed by the precision metric, which is expressed as follows:

$$\text{Precision} = \frac{\text{Number of edge points correctly detected}}{\text{Total number of edge points}} \quad (7)$$

We opted for the precision metric because it does not include false positives, which can be numerous in the set of edges obtained from the region-based segmentation. Indeed, most of these edges are doubled; because they are formed from the two borders of the corresponding adjacent regions (see Fig. 2.e).

B. Visual Results

We start the evaluation of our method by introducing a visual result of the detection according to the two representations then the final segmentation following the relaxation operated on the two sets of contours, by region growing and by edge detection using Canny filter. Figure 2.a shows a range image of the test set, namely abw.test.10. The display is carried out by a rendering procedure, allowing a visualization of the surfaces by the reflection of a simulated light [30] on the surfaces calculated from the raw data. Figure 2.b shows the ground truth of edge detection, calculated from the ground truth of surfaces provided by the ABW database. Figure 2.c shows the edge detection results using the Canny algorithm with the gradient vector composed of the 3 parameters (a, b, c) of the plane equation $z = ax + by + c$. Figure 2.d shows the results of multi-seed region growing with the surface curvature as homogeneity criterion. Figure 2.e shows the edges representing the borders of the surfaces detected by region growing. We note the doubled thickness of such edges contours, because the latter are formed from the two borders of the adjacent surfaces. Figure 2.f shows the final segmentation result expressed by the edges obtained following the relaxation of the two sets C_1 and C_2 (see Section 3).

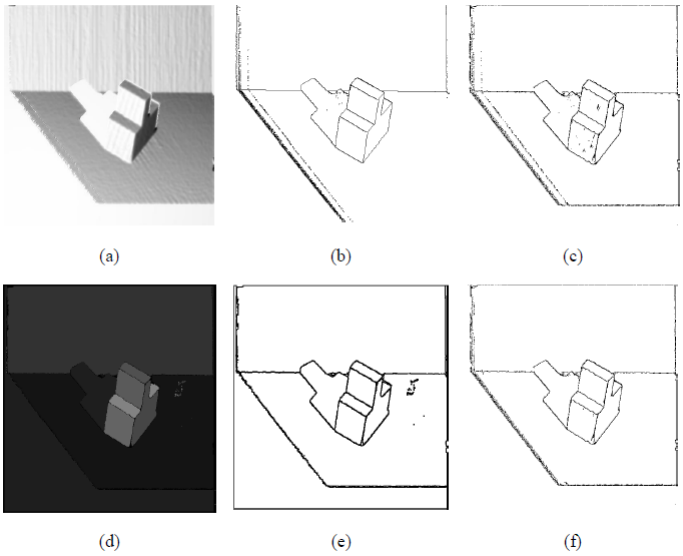

Figure 2. Visual results on an example of range image (abw.test.10)

We notice on figure 2, the significant improvement of the edges obtained in the image 2.f, by comparing them to the edges obtained respectively in the images 2.b and 2.e, and which correspond to the edges obtained respectively by the Canny detector and by the region growing.

C. Quantitative Evaluation

We conducted a series of experiments to show the contribution of each step of the proposed method. First, edge detection by the Canny filter using the gradient based on the parameters of the plan equation and the results are compared with the Canny detector on the raw image data (depths). Then, we compare the results obtained by the cooperation of the two methods: 1) Canny on the parameters of the plan equation, and 2) the region growing by multi-grained region growing on Gaussian curvature as homogeneity criterion. We present in Table I, the precision values obtained on the 30 test images (abw.test.0 ... abw.test.29). We can notice the large gap between the precision values pourusing the raw data, and those using the parameters of the equation of the local tangent plan at every pixel. Figure 2.b shows the ground truth of region-based segmentation provided ABW database. However, we evaluate the obtained edge maps (for both raw data and plan equation parameters) by comparing obtained edges with those obtained following region growing and border extraction. A good matching of the two sets of edges (C_1 and C_2) indicates good detection of edge maps.

TABLE I. Edge detection accuracies of the 30 test images: Results of Canny detector, on the "Raw" data (Raw), and using the coefficients of the equations of the plans (Plan).

Image	0	1	2	3	4
Raw	0,7461	0,6411	0,6917	0,7827	0,6903
Plan	0,9223	0,9543	0,9536	0,9305	0,8921
Image	5	6	7	8	9
Raw	0,7025	0,6856	0,5064	0,7376	0,6573
Plan	0,9225	0,9412	0,9746	0,9289	0,9492
Image	10	11	12	13	14
Raw	0,6029	0,6548	0,7485	0,5925	0,6108
Plan	0,9475	0,9274	0,8991	0,9589	0,9388
Image	15	16	17	18	19
Raw	0,7284	0,7433	0,6418	0,39	0,6271
Plan	0,9448	0,931	0,9361	0,9612	0,9685
Image	20	21	22	23	24
Raw	0,5221	0,5464	0,6085	0,6821	0,6996
Plan	0,9611	0,949	0,9547	0,9072	0,9358
Image	25	26	27	28	29
Raw	0,5095	0,616	0,4875	0,4263	0,4288
Plan	0,9672	0,9265	0,9614	0,9735	0,9472

We notice in Table I that on all the 30 test images, a mean and a standard deviation of respectively 0.6236 and 0.1050 were recorded with the raw data, and a mean and a standard deviation of respectively 0.9422 and 0.0209 with the coefficients of the plan equations. For the evaluation of the relaxation-based cooperation of the two representations of the results, we compared the detection results obtained by Canny before the relaxation and the results after the relaxation by considering the map of edges obtained following region-based segmentation as a reference. The obtained results, introduced in Table II, show the significant improvement in the detection after the relaxation of the results of the two methods, by comparing the obtained results with those of the Canny filter taken individually, even if it operates on the vectorial representation of the image data. For all the images in the ABW database, an average improvement in precision is 3.20%, where values vary between 0.4% and 6.0%, which is considered as significant.

TABLE II. Edge detection comparison on the 30 test images, before and after relaxation of the results.

Image	0	1	2	3	4
Canny	0,9223	0,9543	0,9536	0,9305	0,8921
Relax.	0,9706	0,9725	0,9769	0,9537	0,9526
Image	5	6	7	8	9
Canny	0,9225	0,9412	0,9746	0,9289	0,9492
Relax.	0,9568	0,9774	0,9786	0,9583	0,9719
Image	10	11	12	13	14
Canny	0,9475	0,9274	0,8991	0,9589	0,9388
Relax.	0,9842	0,9632	0,9525	0,9742	0,9657
Image	15	16	17	18	19
Canny	0,9448	0,931	0,9361	0,9612	0,9685
Relax.	0,9688	0,9669	0,989	0,9897	0,9902
Image	20	21	22	23	24
Canny	0,9611	0,949	0,9547	0,9072	0,9358
Relax.	0,9817	0,9928	0,9821	0,9679	0,9712
Image	25	26	27	28	29
Canny	0,9672	0,9265	0,9614	0,9735	0,9472
Relax.	0,9929	0,9659	0,9882	0,9969	0,9896

Introduced results in Table II show the interest of the relaxation. Indeed, matching the results of detection obtained by the filter of Canny on the parameters of the equations of the plans, and the resulted region borders obtained from the region-based segmentation using Gaussian Curvature as homogeneity criterion has allowed to significantly enhancing edge maps for all the test images on the ABW database. However, it should be noted here that the obtained contribution in terms of precision has a consequence on the calculation time, which becomes longer, because the relaxation is based on a meta-heuristic, namely the simulated annealing. Indeed,it is well established in the literature that meta-heuristics are computationally intensive [32].

5. Conclusion

We have presented and evaluated in this paper a new relaxation-based cooperative method for edge detection in range images. The resulting edge detection is obtained according to two different representations, namely by region, using Gaussian curvature as homogeneity criterion, and by edges using plan equation parameters for Canny detection. A relaxation performed on these two detection results has allowed en enhance the final edge map of the processed range images. Indeed, the edge map obtained following the relaxation is more accurate than that obtained by the only Canny detector, even the latter is applied to a refined representation, namely the parameters of the equation of the local plan at each pixel, where they were used to compute the image gradient. Experimental results, whether visual or quantitative, show the strong interest of the relaxation-based combination of the two image representations for a significant improvement of edge detection in range images. Several other types of images, such are medical ones, where regions cloud be defined as objects of interest, could be segmented by the proposed approach. Experimenting our method on such images consists one of our immediate future work.

References

[1] Z. Zhang, "Microsoft kinect sensor and its effect," *IEEE multimedia*, vol. 19, no. 2, pp. 4–10, 2012.

[2] F. Fooladgar and S. Kasaei, "A survey on indoor rgb-d semantic segmentation: from hand-crafted features to deep convolutional neural networks," *Multimedia Tools and Applications*, vol. 79, no. 7, pp. 4499–4524, 2020.

[3] A. K. Tyagi and G. Rekha, "Challenges of applying deep learning in real-world applications. book-challenges and applications for implementing machine learning in computer vision," 2020.

[4] M. R. Jimenez, C. Müller, and H. Pottmann, "Discretizations of surfaces with constant ratio of principal curvatures," *Discrete Comput. Geom.*, vol. 63, no. 3, pp. 670–704, 2020. [Online]. Available: http://www.geometrie.tuwien.ac.at/ig/publications/constratio/constratio.pdf

[5] J. Canny, "A computation approach to edge detection," *IEEE Trans. Pattern Anal. Mach. Intell.*, vol. 8, no. 6, pp. 670–700, 1986.

[6] A. Hoover, G. Jean-Baptiste, X. Jiang, P. J. Flynn, H. Bunke, D. B. Goldgof, K. Bowyer, D. W. Eggert, A. Fitzgibbon, and R. B. Fisher, "An experimental comparison of range image segmentation algorithms," *IEEE transactions on pattern analysis and machine intelligence*, vol. 18, no. 7, pp. 673–689, 1996.

[7] S. Mazouzi and Z. Guessoum, "A fast and fully distributed method for region-based image segmentation," *Journal of Real-Time Image Processing*, vol. 18, no. 3, pp. 793–806, 2021.

[8] J. Poppinga, N. Vaskevicius, A. Birk, and K. Pathak, "Fast plane detection and polygonalization in noisy 3d range images," in *2008 IEEE/RSJ International Conference on Intelligent Robots and Systems*. IEEE, 2008, pp. 3378–3383.

[9] D. Holz and S. Behnke, "Fast range image segmentation and smoothing using approximate surface reconstruction and region growing," in *Intelligent autonomous systems 12*. Springer, 2013, pp. 61–73.

[10] J. Stückler, R. Steffens, D. Holz, and S. Behnke, "Efficient 3d object perception and grasp planning for mobile manipulation in domestic environments," *Robotics and Autonomous Systems*, vol. 61, no. 10, pp. 1106–1115, 2013.

[11] P. Buyssens, I. Gardin, and S. Ruan, "Eikonal based region growing for superpixels generation: Application to semi-supervised real time organ segmentation in ct images," *Irbm*, vol. 35, no. 1, pp. 20–26, 2014.

[12] H. Peng, A. I. Aviles-Rivero, and C.-B. Schönlieb, "Hers superpixels: Deep affinity learning for hierarchical entropy rate segmentation," in *Proceedings of the IEEE/CVF Winter Conference on Applications of Computer Vision (WACV)*, January 2022, pp. 217–226.

[13] C. Dal Mutto, P. Zanuttigh, and G. M. Cortelazzo, "Fusion of geometry and color information for scene segmentation," *IEEE Journal of Selected Topics in Signal Processing*, vol. 6, no. 5, pp. 505–521, 2012.

[14] S. Gupta, P. Arbelaez, and J. Malik, "Perceptual organization and recognition of indoor scenes from rgb-d images," in *Proceedings of the IEEE conference on computer vision and pattern recognition*, 2013, pp. 564–571.

[15] X. Ren, L. Bo, and D. Fox, "Rgb-(d) scene labeling: Features and algorithms," in *2012 IEEE Conference on Computer Vision and Pattern Recognition*. IEEE, 2012, pp. 2759–2766.

[16] N. Silberman, D. Hoiem, P. Kohli, and R. Fergus, "Indoor segmentation and support inference from rgbd images," in *European conference on computer vision*. Springer, 2012, pp. 746–760.

[17] P. Arbelaez, M. Maire, C. Fowlkes, and J. Malik, "Contour detection and hierarchical image segmentation," *IEEE transactions on pattern analysis and machine intelligence*, vol. 33, no. 5, pp. 898–916, 2010.

[18] S. Q. Du, S. J. Tang, W. X. Wang, X. M. Li, Y. H. Lu, and R. Z. Guo, "Pscnet: Efficient rgb-d semantic segmentation parallel network based on spatial and channel attention," *ISPRS Annals of the Photogrammetry, Remote Sensing and Spatial Information Sciences*, vol. V-1-2022, pp. 129–136, 2022. [Online]. Available: https://isprs-annals.copernicus.org/articles/V-1-2022/129/2022/

[19] C. J. Taylor and A. Cowley, "Segmentation and analysis of rgb-d data," in *RSS 2011 workshop on RGB-D cameras*, vol. 90. Citeseer, 2011.

[20] R. Szeliski, *Computer vision: algorithms and applications*. Springer Nature, 2022.

[21] F. F. Pedro and P. H. Daniel, "Efficient graph-based image segmentation," *International journal of computer vision*, vol. 59, no. 2, pp. 167–181, 2004.

[22] Y. Niu, Y. Geng, X. Li, and F. Liu, "Leveraging stereopsis for saliency analysis," in *2012 IEEE Conference on Computer Vision and Pattern Recognition*. IEEE, 2012, pp. 454–461.

[23] J. Strom, A. Richardson, and E. Olson, "Graph-based segmentation for colored 3d laser point clouds," in *2010 IEEE/RSJ international conference on intelligent robots and systems*. IEEE, 2010, pp. 2131–2136.

[24] J. T. Barron and J. Malik, "Intrinsic scene properties from a single rgb-d image," in *Proceedings of the IEEE Conference on Computer Vision and Pattern Recognition*, 2013, pp. 17–24.

[25] A. C. Müller and S. Behnke, "Learning depth-sensitive conditional random fields for semantic segmentation of rgb-d images," in *2014 IEEE International Conference on Robotics and Automation (ICRA)*. IEEE, 2014, pp. 6232–6237.

[26] J. Stückler and S. Behnke, "Efficient dense rigid-body motion segmentation and estimation in rgb-d video," *International Journal of Computer Vision*, vol. 113, no. 3, pp. 233–245, 2015.

[27] S. Liu, Y. Wang, J. Wang, H. Wang, J. Zhang, and C. Pan, "Kinect depth restoration via energy minimization with tv 21 regularization," in *2013 IEEE International Conference on Image Processing*. IEEE, 2013, pp. 724–724.

[28] Z. Zhang, B. Yang, B. Wang, and B. Li, "Growsp: Unsupervised semantic segmentation of 3d point clouds," in *Proceedings of the IEEE/CVF Conference on Computer Vision and Pattern Recognition (CVPR)*, June 2023, pp. 17 619–17 629.

[29] C. Yu, W. Fan, and J. Xiang, "3d point cloud segmentation algorithm based on improved region growing," in *2023 4th International Conference on Computer Engineering and Application (ICCEA)*, 2023, pp. 719–723.

[30] S. Mazouzi, Z. Guessoum, F. Michel, and M. Batouche, "A multi-agent approach for range image segmentation," in *International Central and Eastern European Conference on Multi-Agent Systems*. Springer, 2007, pp. 1–10.

[31] M. Cheribet and S. Mazouzi, "A new adapted canny filter for edge detection in range images," *Jordanian Journal of Computers and Information Technology*, vol. 7, no. 3, 2021.

[32] K. Rajwar, K. Deep, and S. Das, "An exhaustive review of the metaheuristic algorithms for search and optimization: taxonomy, applications, and open challenges," *Artificial Intelligence Review*, vol. 56, 04 2023.

Imene Belloum is Assistant Professor in the Department of Computer Science, 20 Aout 1955 University of Skikda, Algeria.She received her Master degree in computer science in 2012 from Tunis EL Manar unisversity, Tunisia. She is perusing a Ph.D. in computer science and engineering from Abdelhamid Mehri university Constantine, Algeria. Her research field is Computer vision and optimization.

Mourad Bouzenada was born and brought up in Constantine where he was graduated in 1990 at Mentouri University. He began his career as a computer science engineer with mechanical public company. During his seven years with this company he spent most time in the development of applications before returning to university to take a Ph.D. degree in 2008. Currently, he teaches at Mentouri University and he is a member of MISC laboratory. His research interests include computer vision and real-time tracking for augmented reality. He is also interested in the distributed computing aspects of real-time systems. More recently, he studies graph coloring for distribution.

Smaine Mazouzi received his M.Sc. and Ph.D. degrees in computer science from the University of Constantine, respectively in1996, and 2008. He is Professor at 20 Aout 1955 University of Skikda and the Head of AI and DAI team at the LICUS Laboratory (Laboratoire d'Informatique et de Communication de l'Université de Skikda), at the same university. His fields of interest are pattern recognition, machine vision, distributed systems, and computer security. His current research concerns using distributed and complex systems modeled as multi-agent systems in image understanding and intrusion detection. He is the member of several national and international research projects in computer vision and computer security.